Microchemical Journal 190 (2023) 108661

Contents lists available at ScienceDirect

Microchemical Journal

journal homepage: www.elsevier.com/locate/microc

Electrochemical dating of archaeological gold based on repetitive voltammetry monitoring of silver/copper in depth concentration gradients

Antonio Doménech-Carbó [a,*], Fritz Scholz [b], Michael Brauns [c], Sian Tiley-Nel [d], Joosje van Bennekom [e], Ellen van Bork [e], Joaquín Barrio [f], Santiago Martínez-Caballero [g], Arturo Oliver [h], Gustavo Aguilella [i], Betlem Martínez [j], María Teresa Doménech-Carbó [k]

[a] Department of Analytical Chemistry, University of Valencia, Dr. Moliner, 50, 46100 Burjassot (Valencia), Spain
[b] Universität Greifswald, Institut für Biochemie, Felix-Hausdorff Straße 4, 17487 Greifswald, Germany
[c] Curt-Engelhorn-Zentrum Archäometrie gGmbH D6, 3 (OG 3) 68159 Mannheim, Germany
[d] Department of Historical and Heritage Studie, Faculty of Humanities & the University of Pretoria Museums, University of Pretoria, Private Bag X20, Hatfield 0028, South Africa
[e] Rijksmuseum, Department of Metal Conservation and Science, Hobbemastraat 22, 1071ZC Amsterdam, the Netherlands
[f] Departamento de Prehistoria y Arqueología, Universidad Autónoma de Madrid, Avd. Tomás y Valiente 1, 28049 Madrid, Spain
[g] Museo de Segovia, C/ del Socorro, 11, 40003 Segovia, Spain
[h] Museu de Belles Arts de Castelló, Avenida Hermanos Bou, 28. 12003. Castellón de la Plana, Spain
[i] Servicio de Investigaciones Arqueológicas y Prehistóricas, Diputación de Castellón Avda. Hnos Bou 28 (edificio Museu)12003, Castellón, Spain
[j] Servei d'Investigació Arqueològica Municipal de València (SIAM), Polígono Vara de Quart, calle Traginers, Valencia, Spain
[k] Institut de Restauració del Patrimoni, Universitat Politècnica de València, Camí de Vera 14, 46022 València, Spain

ARTICLE INFO

Keywords:
Gold
Dating
Archaeology
Electrochemistry

ABSTRACT

The use of repetitive voltammetry for dating archaeological gold objects is described. The method involves the record of the gold- silver-, and copper-related voltammetric responses obtained for metal nanosamples attached to graphite electrodes immersed into HCl electrolytes. This methodology permits to characterize different electrochemical types representative of different manufacturing techniques. Age estimates are based on the assumption that decuprification/desilvering processes advance with time under reasonably uniform conditions. Age calibration curves covering a range of ca. 2500 years were obtained from a set of archaeological samples from the Mapungubwe Gold Collection at the University of Pretoria Museums, South Africa, the Rijksmuseum of Amsterdam, The Netherlands, the Rheinische Landesmuseum Trier of Mannheim (Germany), the Museu de Belles Arts de Castelló, Spain, the Museu de Segovia, Spain, and the repository of the Servei d'Investigació Arqueològica Municipal de València, Spain.

1. Introduction

Dating metallic archaeological artifacts is an important archaeometric target. It is usually achieved, when associated to organic matter, by dating these components by means of radiocarbon dating. When associated to ceramic materials, dating can be obtained by means of thermoluminescence, obsidian hydration, and rehydroxylation methods [1–3]. However, there are few analytical methods aimed to directly date metals, limited to the use of Meissner superconducting effect in the case of lead [4], and He, U, and Th analysis for gold [5,6]. The practical application of these methods in the archaeological field suffers by the requirement of sample amounts of some hundred milligrams.

In this context, electrochemical methods appear as a plausible technique for dating purposes because of its capability to handle sample amounts at the sub-microgram level. Dating methods for lead [7], copper/bronze [8], and leaded bronze [9] were previously proposed, all based on the voltammetry of immobilized particles (VIMP) methodology. This requires net amounts of sample at the nanogram level extracted from the corrosion patina of metal artifacts [10]. These dating methods are based on the assumption that the objects were submitted to a continuous corrosion process under quasi-uniform conditions so that the both average composition of the metal patina as well as its roughness, crystallinity, porosity, etc. vary with the age.

In the case of gold artifacts, the above scheme cannot be applied due

* Corresponding author.
E-mail address: antonio.domenech@uv.es (A. Doménech-Carbó).

https://doi.org/10.1016/j.microc.2023.108661
Received 14 March 2023; Received in revised form 16 March 2023; Accepted 17 March 2023
Available online 28 March 2023

to the noble character of this metal, which blocks the formation of 'gross' corrosion patinas. However, electrochemical dating methods based on the modification of gold-centered voltammetric responses associated to the formation of surface defects and the adsorption of oxygen functionalities can be proposed [11,12].

Gold is particularly interesting in the archaeological context because of its high material and symbolic value [13–15]. The value of gold as an age marker is obvious because, by virtue of its reluctance to corrosion, the aging processes should be less sensitive to the environmental conditions than other metals [10]. However, several difficulties appear: i) the need of using minimal amounts of sample as far as unique, precious objects are studied; ii) the absence of gross corrosion processes as occurring in copper and bronze; iii) as in the case of other metals, the aging depends not only on the environmental conditions but also significantly on the chemical composition (gold is mainly accompanied by silver and copper [14,15]) and the thermomechanical treatments applied during manufacturing steps [16,17].

The first difficulty can be attended to by using the voltammetry of immobilized particles methodology (VIMP), a solid state technique that permits to analyze sparingly soluble solids at the nanogram level [18,19]. This technique has been widely used in the fields of archaeometry, conservation and restoration [20–22], including the aforementioned methods of metal dating [7–12] and ceramics dating [23], updated in successive reviews [24,25].

One possibility to solve the second problem is based on the fact that metal alloys in general undergo partial release of the less noble components giving rise to decuprification, destannification and dezincation processes [26,27]. Monitoring these processes, however, is made difficult by the existence of very different manufacturing processes resulting in the surface enrichment of noble components [28] and variable concentration profiles associated to plating [29] and other metallographic techniques can occur [30–33]. In fact, although the variation of the Zn/Cu and Sn/Cu ratios in the corrosion patina of bronze and brass alloy was proposed as chronological indicators [34,35], no age calibration methods based on this strategy are available.

Here, we report an approach to solve these problems based on the idea that the variation of the concentration of silver and copper in the subsurface zone of gold artifacts can be monitored via repetitive voltammetry. As described in previous depth profile analysis of bronze [36,37], the application of successive potential scans provides information of increasingly deeper regions of the metal surfaces. The methodology proposed here exploits the well-defined signals recorded for the oxidation of gold, silver and copper appearing in metal nanosamples attached to graphite electrodes in contact with HCl electrolytes. These signals can be interpreted in the light of abundant VIMP literature on copper and bronze [8,9,19–21], silver [38,39], and gold [40,41] and general studies on gold electrochemistry [42–53].

The proposed VIMP methodology was applied to a series of samples originating from the archaeological Mapungubwe Gold Collection at the University of Pretoria, South Africa [54,55] the Rijksmuseum of Amsterdam, The Netherlands, the Rheinische Landesmuseum Trier of Mannheim, Germany, the Museu de Belles Arts de Castelló, Spain, the Muso de Segovia, Spain, and the repository of the Servei d'Investigació Arqueològica Municipal de València, Spain (see Table 1). Complementary experiments were carried out by means of high-resolution field emission scanning electron microscopy (HRFESM-EDX), atomic force microscopy (AFM), and focusing ion beam-field emission scanning electron microscopy (FIB-FESEM). These techniques were applied to several contemporary gold objects. Apart from archaeological gold samples, a series of complementary VIMP experiments were carried out on gold probes submitted to different thermomechanical treatments.

Table 1
Characteristics of the gold samples in this study. MA: Rheinische Landesmuseum Trier, Manheim (Germany); SA: Mapungubwe Collection, University of Pretoria Museums (South Africa), SG: Museo de Segovia (Spain); MC: Museu de Belles Arts de Castelló (Spain); MV: Repository of the Servei d'Investigació Arqueològica Municipal de València (SIAM), Valencia (Spain). In parentheses the percentage (%wt) of silver plus copper estimated from voltammetric data as described in the text.

Sample	Description/Catalogue number	Date
MU01	Gold foil fragment,[SA] Mapungubwe Hill grave area South Africa (SA73, 7.7%)	1200–1290 CE
MU02	Gold foil fragment,[SA] Mapungubwe Hill grave area, South Africa (SA102, 6.8%)	1200–1290 CE
MA01	Globule [MA] (Philippines, 'piloncito') (44%)	900–1200 CE
MA02	Globule [MA] (Philippines, 'piloncito') (64%)	900–1200 CE
MA03	Globule [MA] (Philippines, 'piloncito') (39%)	900–1200 CE
MA04	Lamina[MA] (C6077, 25%)	600–550 BCE
MA05	Lamina[MA] (C3456, 35%)	670–600 BCE
SG01	Bracelet,[SG] Coca archaeological site (A-18328–3.1, 45%)	450 BCE
SG02	Bracelet,[SG] Coca archaeological site (A-18328–2.2, 44%)	450 BCE
MC01	Ingot,[MC] Santa Llúcia, Alcalà de Xivert (SLL18-1 h, 30%)	575 BCE
MC02	Ingot,[MC] Santa Llúcia, Alcalà de Xivert (SLl18-1a, 31%)	575 BCE
MC03	Ingot,[MC] Santa Llúcia, Alcalà de Xivert (SLl18-1c, 30%)	575 BCE
MC04	Ingot,[MC] Santa Llúcia, Alcalà de Xivert (SLl18-1e, 29%)	575 BCE
MC05	Ingot,[MC] Santa Llúcia, Alcalà de Xivert (SLl18-1 g, 28%)	575 BCE
MC06	Earring,[MC] Puig de la Nau, Benicarló (MC1676, 55%)	400–375 BCE
MC07	Plate,[MC] Borriol, Tossalet de les Forques (MC0224, 47%)	100 BCE
MC08	Roman Needle,[MC] Hostalots de Villanueva de Alcolea (MC2373, 16%)	3th-4th CE
MV01	Gold embroidery, Roman age, Valencia, (MIS004 U.E. 1389,1.6%)	ca. 100 CE
MV02	Gold embroidery, Califal period, Valencia (11ALM00 U.E. 10793, 2.0%)	ca. 1000 CE

2. Experimental details

2.1. Samples

Archaeological gold samples were taken from the Mapungubwe archaeological gold Collection at the University of Pretoria Museums, South Africa (MU01-MU02), the Rijksmuseum of Amsterdam, The Netherlands, the Rheinische Landesmuseum Trier of Mannheim, Germany (MA01-MA05), the Museu de Belles Arts de Castelló, Spain MC01-MC05), the Museo de Segovia (SG01-SG02) and the repository of the Servei d'Investigació Arqueològica Municipal de València, Spain (MV01-MV02). These were complemented by recent gold objects (Z01-Z05). The relevant properties of these objects are listed in Table 1.

A second series of gold samples were taken from a series of objects from the Rijksmuseum of Amsterdam (RM01-RM14) several of which (without historical or archaeological value) were submitted to heating at 800 °C in oven, molten, or hammer, as summarized in Table 2. These samples were used to test the influence of the different thermomechanical treatments on the voltammetric response and, hence, on dating. The treated objects were submitted to two sampling runs. The former, immediately of the treatment and stabilization at room temperature, was performed in October 2022, 10 days after the application of the thermomechanical treatments. The second sampling on the same objects was carried out four months later (20th January 2023). In both cases, the samples were submitted by mail to the University of Valencia where the voltammetric measurements were performed just five days after the sampling.

2.2. Instrumentation and methods

Voltammetric experiments were performed at 298 ± 1 K using a CH I660 potentiostat (Cambria Scientific, Llwynhendy, Llanelli UK). Sample-modified graphite working electrodes were used as working electrodes. A platinum wire auxiliary electrode and an Ag/AgCl (3 M

Table 2
Characteristics of the gold samples from private repositories (Z) and prepared in the Rijksmuseum Amsterdam (RM). H: hammered; Q: heating in oven at 800 °C; M: molten; MS: Molten and treated with sulfuric acid. In parentheses the percentage (%wt) of silver plus copper estimated from voltammetric data as described in the text.

Sample	Description	Fabrication date	Treatment
Z01	Ring (25%)	1988	None
Z02	Religious medal (38%)	1902	None
Z03	Religious medal (17%)	1980	None
Z04	Ring (25%)	1950	None
Z05	Religious medal (26%)	1903	None
RM01	Bracelet (40%)	ca. 1950	None
RM02	Coupe (10%)	17th century	None
RM03	Bracelet (10%)	ca. 1950	Q
RM04	Bracelet (16%)	ca. 1950	M
RM05	Earring (20%)	1990	None
RM06	Pin Zeeuws (5%)	ca. 1850	None
RM07	Aigrette (42%)	17th century	None
RM08	Earring (24%)	1990	M
RM09	Earring (36%)	1990	Q
RM10	Ring (32%)	2022	None
RM11	Pin Zeeuws (8%)	ca. 1850	M
RM12	Pin Zeeuws (10%)	ca. 1850	Q
RM13	Earring (30%)	1990	H
RM14	Earring (30%)	1990	MS

NaCl) reference electrode completed the three-electrode electrochemical cell. Air-saturated 0.10 M HCl aqueous solutions optionally deaerated by bubbling Ar during 10–15 min were used as electrolytes. Faber-Castell HB (2 mm diameter) were used as working electrodes. Sampling was performed by gently pressing graphite bars onto plain areas of the archaeological objects as previously described [11,12]. The graphite electrodes of the different suppliers provided small but consistent differences in their voltammetric responses. In the following, data will be referred to the former working electrodes.

FIB-FESEM experiments were performed with ion beam Zeiss (Orsay Physics Kleindiek Oxford Instruments), model Auriga equipment, operating conditions: voltage, 30 kV and current intensity, 500 μA and 20nA in FIB to generate the focused beam of Ga ions. The Ga beam impacts perpendicularly on the plane of the vertical wall of the trench by tilting the stage 54° where the object is placed. These areas were previously coated with a Pt layer with a thickness of 300 nm in an area of (8 × 10) μm. FESEM images were acquired at a voltage of 2 kV. HRFESM-EDX experiments were carried out using a Zeiss (Orsay Physics Kleindiek Oxford Instruments) model GeminiSEM 500 with an Oxford-Instrument X-ray microanalysis controlled by the Aztec software. Operating conditions were: voltage 5 kV, working distance of 6–7 mm. The ZAF method was followed to correct the interelemental effects in the semi-quantitative microanalysis; counting time 100 s. The secondary electron images and X-ray spectra were obtained in cross-sections acquired in the spot mode.

AFM experiments were performed with a multi-mode AFM (Digital Instruments VEECO Methodology Group, USA) with a NanoScope IIIa controller and equipped with a J-type scanner (max. scan size of 150 × 150 × 6 μm). An oxide-sharpened silicon nitride probe Olympus (VEECO Methodology Group, model NP-S) with a V-shaped cantilever configuration was used to study the topography of a gold-coated AT-cut quartz crystal immersed into 0.10 M HCl electrolyte in the contact mode.

3. Results and discussion

3.1. Voltammetric pattern

Fig. 1 shows the linear potential scan voltammetric (LSV) response of graphite electrodes modified with gold samples RM05 (earring fabricated in 1990) and Z03 (medal fabricated in 1980) in contact with 0.10

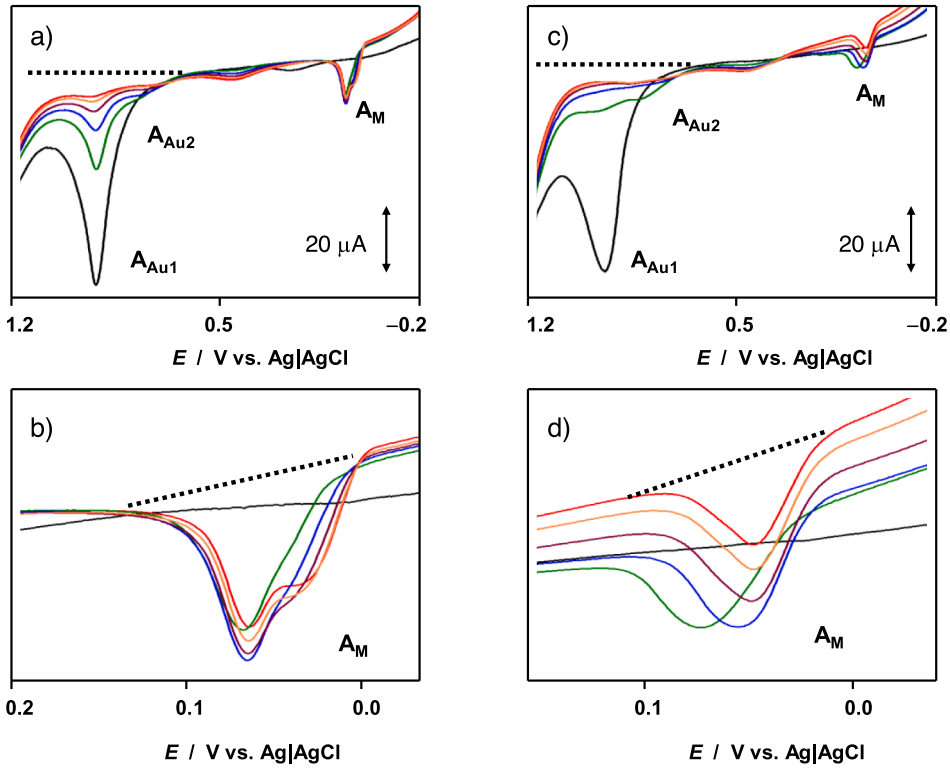

Fig. 1. Successive LSVs of gold samples attached to graphite electrode in contact with air-saturated 0.10 M HCl. a,b) sample RM05; c,d) sample Z03. The arrows mark the variation from the 1st to 6th scans. Dotted lines are examples of the baselines used for peak current measurements. a,c) Entire LSVs initiated at −0.25 V vs. Ag/AgCl in the positive direction and b,d) detail of the A_M region; potential scan rate 50 mV s^{-1}.

M HCl when six positive-going potential scans are successively applied. The first potential scan yields a main anodic peak at ca. 0.95 V vs. Ag/AgCl ($A_{Au1}(1)$) preceded by tall a peak at 0.05 V ($A_M(1)$) and a weak shoulder at ca. 0.85 V ($A_{Au2}(1)$). In the second and subsequent scans, the height of signal A_{Au1} decreases. The opposite behavior was also observed for the peak A_M which in most cases appears as two strongly overlapping peaks, whose height tends to a limiting value. The signal A_{Au2} has a peculiar behavior in successive potential scans, it initially increases but further progressively decreases.

These features can be seen in Figure S.1 of Supplementary Information, where the region of potentials where the A_M signal appears is depicted for samples Z01 (ring fabricated in 1988) and MA02 (Philippine 'piloncito', a globule of ca. 5 mm diameter used as currency in the Indopacific area between 900 and 1200 CE), accompanied by the variation of the peak currents in successive scans. These peak currents were measured using the criteria illustrated in Fig. 1 and Figure S.1.

To interpret these features it has to be considered that the sample-modified electrodes consist of a set of metal sheets of micrometric size (typically 1–5 μm-sized) adhered to the surface of the graphite electrode. Typical SEM images of the sample-modified electrodes can be seen in Fig. 2a,b. The electrochemical A_{Au1} can be described in term of the oxidative dissolution of gold [41] to Au(III)-chloride complexes, generically represented by the equation,

$$Au_{solid} + xCl^-_{aq} \rightarrow Au^{III}Cl^{(3-x)+}_{x,aq} + 3e^- \quad (1)$$

This process is sensitive to structural factors [46] and the attack of the metal surface by reactive species [49–51]. The repetition of the anodic potential inputs produces the progressive delamination of the gold sheets. This is illustrated in SEM images in Fig. 2c,d where a clear narrowing of the gold flakes extracted from sample Z02 (a gold medal fabricated in 1902) is observed. The images correspond to gold sheets adhered to a graphite plate before and after application of a potential step of 1.25 V for 5 min in 0.10 M HCl. Following literature [47,48,52], the process A_{Au2} can be assigned to the oxidative dissolution of active gold sites. These can be viewed as coordinatively unsaturated centers associated to surface and subsurface defect sites.

Finally, the process A_M can be described as the oxidation of copper and silver (M = Ag, Cu) to the corresponding of M(I) chlorides. As far as these are scarcely soluble compounds, the process A_M can be considered as a solid-to-solid M/MCl interconversion,

$$M_{solid} + Cl^-_{aq} \rightarrow MCl_{solid} + e^- (M = Ag, Cu) \quad (2)$$

competing with the formation of M−chloride complexes in solution and/or the formation of other solids such as $CuCl(OH)_3$). Cycling the potential determine the alternative formation of MCl and M solid deposits so that, in contrast with the above Au-related processes, the peak current tends to a limiting constant value after few potential cycles. The coexistence of copper- and silver-localized voltammetric signals was confirmed by experiments using acetate buffer as the electrolyte. Here, multiple peaks appear at potentials between 0.0 and 0.4 V while the gold peaks become considerably lowered (see Supplementary information, Figure S.2).

The density of observed flakes in SEM images can be correlated with the charge passed under the voltammetric peaks (see Supplementary Information, Appendix A.1).

3.2. Surface and subsurface analysis

The above electrochemistry was consistent with the examination of the surface and subsurface region of gold objects at the nanoscopic scale. Figure S.3 in Supplementary Information shows the amplitude error channel graphs and topographic AFM images at the micrometer scale of a gold-coated AT-cut quartz crystal immersed into 0.10 M HCl before and after application of a potential of 1.25 V for 2 min. The gold surface shows initially a certain roughness with peak-shaped features and a smoothed surface after application of the oxidation potential. This surface smoothening is due to the preferential oxidative dissolution of gold asperities, as observed after attack by OH radicals [47–51].

Figure S.4a shows the secondary electron image of the obverse of object Z02 (a medal fabricated in 1902) marking the smooth area in which was performed a 50 × 50 μm trench by FIB to perform EDX depth analysis (vide infra). Figure S.4b shows an enhanced image of that trench with detail of the spots where the elemental depth profiling using the X-ray microanalysis was carried out. Trenches performed in rough regions of the medal (Figure S.4c,d) show the Pt protective coating and the presence of cracks and crevices in the subsurface zone. As already

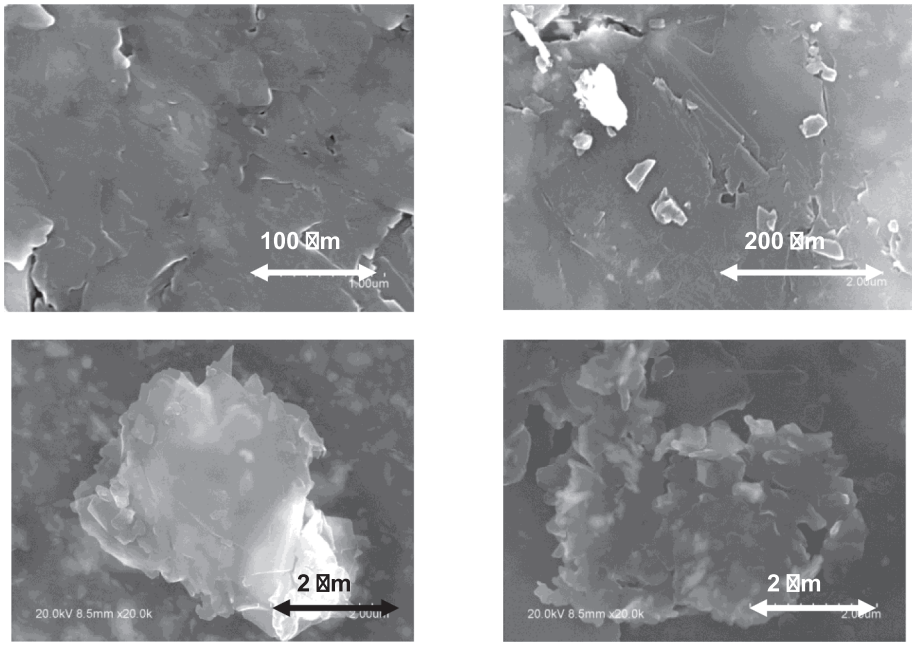

Fig. 2. A,b) secondary electron images of gold plates from a medal fabricated in 1902 (sample z02) abrasively transferred onto a graphite plate in contact with 0.10 M HCl at different magnifications. c,d) images of a gold lamina c) before and d) after application of a potential step of 1.25 V for 5 min.

reported [11], EDX data indicate that the oxygen/metal ratio sharply decreases in the upper 200 nm surface, whereas the Ag/Au and Cu/Au ratios increase progressively from low values in the external region to a limiting value reached at ca. 10 μm depth. This is illustrated in Figure S.5 where the atomic Ag/Au and Cu/Au ratios determined in FIB-FESEM experiments in a 20 × 20 μm trench excavated in sample Z02 are depicted.

The values of the charge passed in LSV experiments, typically around 20–100 μC for the A_M peak, are consistent with the SEM data in Fig. 2 and Figure S.4 (see a detailed calculation in Supplementary Information, Annex A.1) suggesting the attachment of gold flakes of averaged dimensions of 5 × 5 × 1 μm onto the graphite electrode with an averaged density of 1.6×10^{-4} flakes μm^{-2}.

Interestingly, the variation of such ratios can be correlated with the peak current variations obtained in successive potential scans. To rationalize voltammetric data, let us assume that the sample abrasively transferred onto the graphite electrode surface consists of a set of n metal flakes of each one having an area S_j and thickness d_j (see Figure S.6 in Supplementary Information to schematize the sampling process). Taking into account that the processes A_{Au1}, A_{Au2} determine the oxidative dissolution of gold, each potential scan will determine the dissolution of a layer of a thickness $\delta_j(N)$ ($<d_j$) of each flake. If we perform successive anodic scans there will be an oxidative de-lamination of gold. The charge passed during the N^{th} anodic scan for the Au- and Ag- plus Cu-centered oxidation signals, $q_{Au}(N)$, $q_M(N)$, is:

$$q_{Au}(N) = 3F\sum_{j=1}^{n} S_j(N)\partial_j(N)\rho_j(N)f_j^{Au}(N) \quad (3)$$

$$q_M(N) = F\sum_{j=1}^{n} S_j(N)\partial_j(N)\rho_j(N)f_j^{M}(N) \quad (4)$$

where $\rho_j(N)$ represents the average density (g cm^{-3}) of the delaminated region and $f_j^{Au}(N)$ the mass fraction of Au in the j-flake. Notice that the value of $q_{Au}(N)$ has to be calculated as the sum of the areas under the voltammetric peaks A_{Au1} and A_{Au2}. Assuming for simplicity that the sample-modified electrode is formed by n identical laminas of an averaged area S and an averaged thickness d, and that S does not vary in successive oxidative delaminations, the charge passed at the N^{th} scan can be approximated by:

$$q_{Au}(N) = 3FnS\delta(N)\rho(N)f^{Au}(N) \quad (5)$$

$$q_M(N) = FnS\delta(N)\rho(N)f^{M}(N) \quad (6)$$

Our voltammetric data indicated that the charge passed under the peaks A_{Au1} plus A_{Au2} and the peak A_M are proportional to the corresponding peak currents measured using the baselines depicted in Fig. 1 and Figure S.1 (see Figure S.7 in Supplementary information). Accordingly, Eqs. (5) and (6) can be rewritten as:

$$i_{Au}(N) = g_{Au}n\delta(N)\rho(N)f^{Au}(N) \quad (7)$$

$$i_M(N) = g_M n\delta(N)\rho(N)f^{M}(N) \quad (8)$$

where g_{Au}, g_M, represent electrochemical constants depending on the conditions used in the voltammetric experiments (g = f(electrochemical rate constant, number of electrons, coefficient of electron transfer, potential scan rate, etc.)). To estimate the depth reached in the oxidative delamination of gold flakes at the N^{th} scan, we can use the total charge passed, $Q_{Au}(N)$ ($= q_{Au}(1) + q_{Au}(2) + ...q_{Au}(N)$) or, equivalently, the cumulative peak current, $I_{Au}(N)$ ($= i_{Au}(1) + i_{Au}(2) + ...i_{Au}(N)$). This last quantity can be expressed as:

$$I_{Au}(N) = g_{Au}\sum \delta(1)\rho(1)f^{Au}(1) + ... + \delta(N)\rho(N)f^{Au}(N) \quad (9)$$

where $\delta(1) + \delta(2) + ... + \delta(N) = z$, the depth reached at the N^{th} voltammetric scan. Since $I_{Au}(N)$ can be considered as representative of the average density and the average molar fraction of gold existing between the surface ($z = 0$) of the object and the depth z, $I_{Au}(N)$ can be taken as a rough measure of that depth. In cases where the gold content was high, one can assume that both the density of the metal phase and the mass fraction of gold remain essentially constant throughout the laminas so that:

$$I_{Au}(N) \approx g_{Au}n\rho(z)f^{Au}(z)\sum \delta(1) + ... + \delta(N) = g_{Au}nz\rho(z)f^{Au}(z) \quad (10)$$

Accordingly,

$$\frac{i_M(N)}{I_{Au}(N)} \approx \frac{g_M n\rho(z)f^{M}(z)}{g_{Au}nz\rho(z)f^{Au}(z)} = g\frac{f^{M}(z)}{f^{Au}(z)} \quad (11)$$

where $g = g_{Ag}/g_{Au}$ is an electrochemical constant. Equation (11) expresses the depth variation of the ratio between the mass (or molar) fractions of Ag plus Cu and Au. For our purposes, the relevant point to emphasize is that the variation of $i_M(N)$ with $I_{Au}(N)$ can be taken as approximately representing the depth variation of the Ag plus Cu concentration in the gold flakes. Ideally, for a sufficiently large number of electrochemical runs, the limiting value of the $i_M(N)/I_{Au}(N)$ ratio will provide the bulk composition of the metal phase:

$$\left[\frac{i_M(N)}{I_{Au}(N)}\right]_{N\to\infty} = g\frac{f^{M}(\text{bulk})}{f^{Au}(\text{bulk})} \quad (12)$$

Our experimental data yields $i_M(N)$ vs. $I_{Au}(N)$ curves as illustrated in Fig. 3 for samples Z01 (ring fabricated in 1988), MA03 (Philippine 'piloncito' dated back between 900 and 1200 CE), and MC01 (Iberian sheet dated back to 575 BCE). One can see that experimental data define an initial s-shaped growth region followed by a more or less smooth decrease. These results suggest, in agreement with FIB-FESEM data (see Supplementary Information, Figure S.5) and literature [15,56–59], that the concentration of Ag and Cu is depleted near the surface of the gold object. The depth of the gold-enriched surface layer, in general very thin [56,58], depends on several aspects including alloy composition (the higher the less noble metal content, the higher its possible depletion) and, if it is the case, burial conditions [15]. Similar copper depletion has been repeatedly reported in silver coins [22,60–63], where frequently copper has been completely stripped out at the subsurface regions [22].

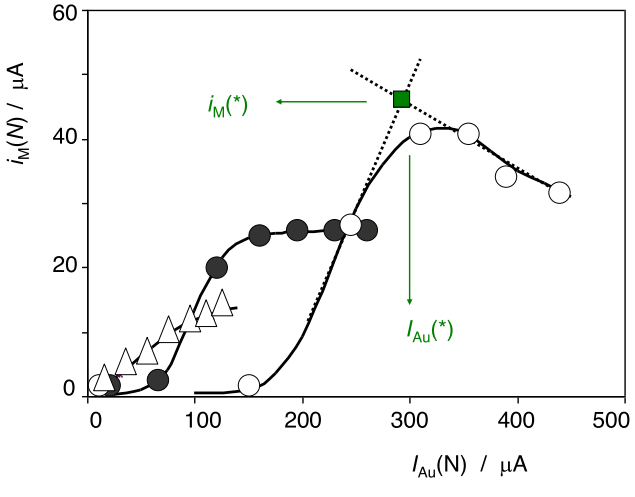

Fig. 3. Variation of $i_M(N)$ on $I_{Au}(N)$ for samples Z01 (circles), MA03 (solid circles), and MC01 (triangles). Continuous lines correspond to the connection of experimental data points by logistic functions. The dotted lines mark the straight tendency lines approximately defined by the 'surface' and 'bulk' portions of data. Their intersection (square) was taken as the reference for compensating the differences in net amount of sample transferred onto the electrode surface in replicate experiments and (at least partially) the different (Ag plus Cu)/Au proportions in the metallic objects under study.

Accordingly, the initial rising portion of the $i_M(N)$ vs. $I_{Au}(N)$ curves can be seen as representative of the sharp gradient of copper plus silver concentration in the external layer of the gold object. These 'subsurface' data can reasonably be fitted logistic functions, as illustrated in Fig. 3. The 'bulk' data, however, varies from rapidly decaying to almost horizontal or smooth rising curves, as can also be seen in Fig. 3. This tendency is also clearly reflected in $i_M(N)$ vs. N curves as depicted in Figure S.8 of Supplementary Information. In these figures one can see that, apparently, the variation of $i_M(N)$ with the depth (represented either by $I_{Au}(N)$ and N) tends to be smoother on increasing the object age. This provides a qualitative dating criterion.

Graphs such as in Fig. 3 and Figure S.8, however, cannot be directly compared because the values of $i_M(N)$ depend on the net amount of gold sample transferred onto the electrode surface, a well-known feature in VIMP [19–21]. To compensate this effect, generalized curves can be constructed taking peak currents normalized to a point (marked by an asterisk in Fig. 3) defined by the intersection between the straight lines which approximate the rising ('subsurface') and decaying ('bulk') regions of the $i_M(N)$ vs. $I_{Au}(N)$ curve, as is illustrated in Fig. 3. The coordinates of this point, $i_M(*)$, $I_{Au}(*)$, permit to built generalized $i_M(N)/i_M(*)$ vs. $I_{Au}(N)/I_{Au}(*)$ curves such as depicted in Figure S.9 (Supplementary Information) for sample MA01. Three different $i_M(N)$ vs. $I_{Au}(N)$ curves obtained from replicate measurements are depicted in Figure S.9a. After normalization, all three curves reduce to a unique $i_M(N)/i_M(*)$ vs. $I_{Au}(N)/I_{Au}(*)$ curve as illustrated in Figure S.9b. As will be further discussed, these generalized curves also compensate –at least partially- the effect of the differences in the proportion of less noble metals on comparing different objects (see below).

3.3. Composition and manufacturing: Electrochemical types

A precondition for dating purposes is to elucidate the influence exerted by the composition and manufacturing type of the gold object in the voltammetric response. Ideally, as previously noted, the bulk composition of the metal object can be obtained as the limiting value of the $i_M(N)/I_{Au}(N)$ ratio when $N \rightarrow \infty$. Since this limiting value offers considerable uncertainty, the bulk metal composition was approximated taking the ratio between the limiting value of $i_M(N)$, submitted to lower uncertainty in representations such as in Fig. 3, Figure S.8 and S.9, and the $i_{Au}(1)$ value. Tables 1 and 2 summarizes the silver plus copper percentage of the studied samples estimated from voltammetric data taking as a reference sample Z01 which nominally contains 25 wt% Ag.

The voltammetric pattern is sensitive to the manufacturing, as judged by the appearance of different LSV profiles in different samples of similar age. For practical purposes, we defined six electrochemical types based on the profile of the A_{Au1} signal in the first positive-going potential scan. Fig. 1a shows an example of the type I, characterized by the appearance of a unique, sharp A_{Au1} signal. The type II, exemplified in Fig. 1c, is characterized by a wider signal A_{Au1}. Fig. 4 shows representative examples of the electrochemical types III to VI. Type III voltammograms, exemplified by that of sample MU02 (gold globule from the Mapungubwe Hill site dated back to 1200–1290 CE, Fig. 4a), are characterized by a shoulder ca. 0.8 V preceding the signal A_{Au1}. In the voltammograms of type IV, the signal at ca. 0.8 V appears as a more or less intense, but separate peak, as can be seen in Fig. 4b for sample RM06 (pin zeeuws fabricated ca. 1850 CE). The type VI is characterized by an isolated A_{Au1} peak which is preceded by prominent signals around 0.6 V, as can be seen in Fig. 4c for sample RM01 (bracelet fabricated ca. 1950 CE). The electrochemical type V is defined by a broad A_{Au1} peak followed by a shoulder at more positive potentials (between 1.1 and 1.2 V).

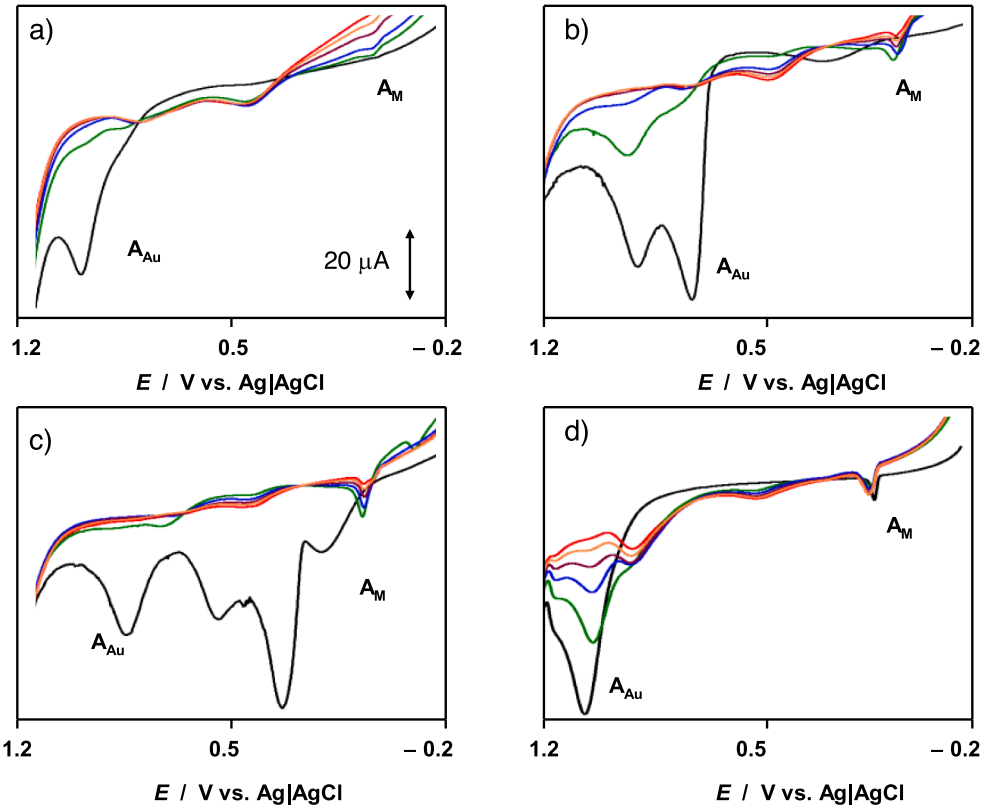

Fig. 4. Repetitive voltammetry on gold samples a) MU02 (gold globule from the Mapungubwe Hill site dated back to 1200–1290 CE), b) RM06 (Pin Zeeuws fabricated ca. 1850 CE), c) RM01 (bracelet fabricated ca. 1950 CE), d) MC08 (needle of Roman age from the Hostalots de Villanueva de Alcolea site, dated back to 3th-4th CE). LSVs recorded in conditions such as in Fig. 1.

This is exemplified by sample MC08 (needle of Roman age from the Hostalots de Villanueva de Alcolea site, dated back to 3th-4th CE) in Fig. 4d.

The differences between the electrochemical types I-VI can be attributed to differences in the manufacturing type. These result in gold surfaces with different preferred crystallographic orientations and defect sites which, in agreement with literature [46–48], produce gold oxidation signals at different potentials. In the case of type VI samples, the sharp signals ca. 0.6 V can be assigned to the accumulation of Ag in the surface, as judged by the electrochemistry of ancient silver objects [25,38]. For our purposes, the relevant aspects to emphasize are that: i) voltammetric data permits to discriminate between different manufacturing techniques, and ii) as will be discussed in the next section, these differences result in different aging patterns.

The variation with the age of the object on the peak potential of the main oxidation peak of gold in the first scan, $E_p(A_{Au1}(1))$ is illustrative of the above issues. This can be seen in Figure S.10 in Supplementary Information, where voltammetric data from samples in this study are accompanied by those previously reported [11,12]. One can see that the voltammetric types IV and VI can reasonably fitted to a smooth polynomial variation of the peak potential with the age clearly differing from that apparently defined by samples of the type V (Figure S10a). The majority of the type V samples are coins, while types IV and VI correspond to rings and earrings. The samples of the types I, II, and III are distributed in an intermediate band of the in the $E_p(A_{Au1}(1))$ vs. age diagram. These samples include ingots and globules as well as rings, pins, earrings, and bracelets.

3.4. Dating

There are different voltammetric features able to be used for dating purposes. These include the peak potential of the process A_{Au1} [11,12] whose variation with the age is illustrated in Figure S.10. A second age marker is defined in Figure S.11. Here, the variation of the accumulated peak current $I_{Au}(N)$ is plotted vs. the scan number N taken as a continuous variable. In all cases, experimental data can satisfactorily be fitted to a function of the type $I_{Au}(N) = aN^b$, a and b being fixed, sample-characteristic parameters. Our data reveal a general tendency to increase the b-exponent with age (see Figure S.12), but there is large dispersion nod no clear separation between the different electrochemical types. As can be seen in Figure S.12, the b values of the thermally treated samples show large variability.

A third quantitative criterion for dating can be obtained from the generalized $i_M(N)/i_M(*)$ vs. $I_{Au}(N)/I_{Au}(*)$ curves in Figure S.9. The essential idea is that the variation of Ag plus Cu concentration with depth must vary with the age. In principle, these elements will form oxidized compounds on the surface of the object, one significant fraction of which is being released as soluble salts. This feature determines the aforementioned surface gold enrichment [17,56–59], and the generation of a more or less sharp concentration gradient in the subsurface region. Under fixed environmental conditions, the oxidation and removal of Ag and Cu will proceed uniformly and will be accompanied by the migration of Ag and Cu from the metal bulk to the surface of the object. The concentration gradient can be measured as the slope of the generalized curves in the almost linear rising portion of the $i(N)/i_M(*)$ vs. $I_{Au}(N)/I_{Au}(*)$ curves.

In principle, this generalized slope must attenuate –but no necessarily compensate- the differences in the composition of the metal. The slope will be also sensitive to the metallographic structure, and can be notably influenced by gilding or other processes produced during the objects' manufacturing [27,28]. Additionally, the Ag plus Cu concentration gradient will depend on the type and rate of environmental aggression as well as possible surface inhomogeneities due to handling, dust, cleaning, etc. These last factors, as well as the adsorption of oxygen species [31,43] can also influence the voltammetric response [11,12].

This variability is reflected in the voltammetric pattern so that different calibration graphs can be constructed for each electrochemical type. This can be seen in Fig. 5, where the slope (SL) of the initial almost-linear portion of the $i_M(N)/i_M(*)$ vs. $I_{Au}(N)/I_{Au}(*)$ curves is plotted vs. the age of the objects.

Data on untreated gold samples reveal an unambiguous tendency to decrease the Ag plus Cu concentration gradient with the age of the tested artifacts. This permits the built of separate calibration graphs for the different electrochemical types. These general tendencies reflect the common tendency to decuprification and desilvering resulting in gold surface enrichment.

Remarkably, as occurred with the b-exponent and peak potential data, the 'very young' samples, those submitted to heating (RM03, RM09, and RM12) or melting (RM04, RM08, and RM11), exhibit low SL values, apparently corresponding to much older untreated specimens. Interestingly, these 'very young' specimens are characterized by the appearance in the first anodic scan of a peak at ca. −0.10 V (A_M*) preceding the Ag plus Cu stripping peak A_M at ca. 0.0 V. This feature, which can be seen in Figure S.13 (Supplementary Information) is absent in all other tested samples (even in 'young' objects 30–50 year old) and suggests that there is a relatively large concentration of Ag plus Cu in the surface of these 'very young' objects.

Remarkably, the repetition of the voltammetric measurements on the 'very young' objects five months after their 'reset', results in a decrease of the intensity of the peak A_M* and an increase of the SL value estimated from the $i_M(N)/i_M(*)$ vs. $I_{Au}(N)/I_{Au}(*)$ curves. This can be seen in Figure S.14 of Supplementary information where the repetitive voltammetry of sample RM08 after 15 days and after five months of its melting are shown accompanied by the respective $i_M(N)$ vs. $I_{Au}(N)$ representations. The value of SL increased from clearly in this time interval in agreement with the initial rising portion of the calibration graph in Fig. 5.

These features can be interpreted on considering that the depletion in copper and silver from the surface of gold alloy objects can occur during manufacture and further by leaching in the post-depositional environment [64–66]. On the other hand, studies on interdiffusion and reactions in thin film systems [67] dealing with the hardening of dental gold alloys [68] aging of gold films [69], and surface enrichment of gold alloys [70], underline the balance between grain boundary or defect enhanced diffusion and 'bulk' or lattice diffusion. In fact, certain manifestations of

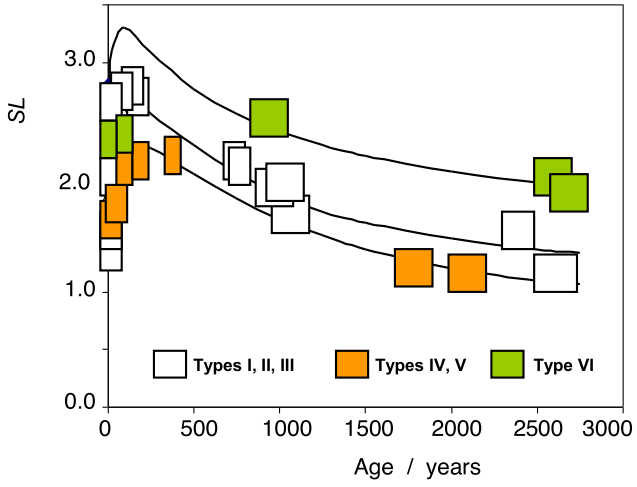

Fig. 5. Calibration graph based on the slope of the central, linear-like region in the generalized $i_M(N)/i_M(*)$ vs. $I_{Au}(N)/I_{Au}(*)$ representations obtained from voltammetric data such as in Fig. 1 for 'ordinary' samples (circles) and treated samples (grey circles). The continuous lines represent exponential-type curves approaching the tendency lines defined by experimental data for the different electrochemical types.

rapid gold surface enrichment, reflected in concentration profiles, have been observed in the range of days-months for gold diffusion in polycrystalline silver films [67] and even in few hours for low gold alloys in contact with artificial saliva [70].

Modeling the observed variation of the concentration gradient with the age is difficult due to the need of considering (at least) two coupled processes: the diffusion (both grain boundary and lattice) of Ag and Cu from the metal bulk to the surface, and the oxidation and release of these elements in the external region of the object. Both desilvering and decuprification may result from the action of local galvanic elements, where Ag and Cu are oxidized parallel to the reduction of oxygen on gold atoms. Since oxygen reduction on gold is catalyzed by active gold sites on the surface, there is possibly an accelerating effect: aging causes an increase of surface concentration of active gold sites, and this increase may enhance the oxygen reduction and thus the Ag and Cu oxidation. Still, the rate of desilvering and decuprification is probably limited by the diffusion of Ag and Cu in gold. Of course, grain boundary diffusion may also occur (at a higher rate than volume diffusion), and here again, the surface corrosion may create better accessible grain boundaries [25].

The shape of the $I_M(N)$ vs. $I_{Au}(N)$ curves (Fig. 3 and Figure S.9) suggests that in recently manufactured objects there is a maximum concentration of Ag plus Cu in the subsurface region descending smoothly towards the external surface as a result of gold enrichment during the fabrication. In these 'very young' objects, the concentration gradient increases rapidly with time because the rate of Ag plus Cu removal exceeds the diffusion rate of these elements from the object bulk. After a certain time, the diffusion becomes rate-determining and this result in the progressive lowering of the concentration gradient defining the descending branches in Fig. 5.

The current results illustrate the capability of the VIMP for providing archaeometric information. The current depth profile analysis suggests that surface profiling method (SIMS or laser ablation spectroscopy) can also be applied for dating purposes, at least in the case of less precious objects.

4. Conclusions

The voltammetric response of gold nanosamples attached to graphite electrodes in contact with 0.10 M HCl permits: i) the grouping of samples on different electrochemical types representative of different manufacturing methods; ii) establishing depth profiles of the concentration of copper and silver to assess subsurface migration during aging; iii) determining different aging patterns and defining different age markers using distinct voltammetric parameters. Among them, age determination based on determining the vertical concentration gradients of copper and silver minority constituents of gold at the gold subsurface region caused by corrosion processes offers the lower data dispersion.

Application of a repetitive voltammetry strategy to copper- and silver-localized signals permits building a satisfactory calibration graph covering a period of ca. 2500 years. Given the low amount of required sample, restricted to the nanogram level, the proposed method is of application in different archaeological contexts. In particular, the method may be of great advantage to reconstruct the history of making gold items, when they have been altered by adding new parts over time, as it is known to have been the case of many precious gold objects like the Imperial Crown of the Holy Roman Empire, and other crowns. Future studies should be directed on other systems: silver may be another candidate where decuprification may lead to a dating method. We could also imagine that a similar approach may be used for the dating of minerals, provided that depth profiles can be sampled.

Declaration of Competing Interest

The authors declare that they have no known competing financial interests or personal relationships that could have appeared to influence the work reported in this paper.

Data availability

Data will be made available on request.

Acknowledgments:

Grant PID2020-113022GB-I00 funded by MCIN/AEI/10.13039/501100011033 and by "ERDF A way of making Europe", by the "European Union frame is gratefully acknowledged. The authors wish to thank Mr. Manuel Planes, Dr. José Luis Moya and Mrs. Alicia Nuez Inbernón, technical supervisors of the Electron Microscopy Service of the Universitat Politècnica de València and Arno Brauns for organizing the ring from Hermeskeil and the trust of the responsible leadership of the Rheinische Landesmuseum Trier, Dr. Marcus Reuter and the Universität des Saarlandes, Prof. Dr. Sabine Hornung. In addition, to Maggie Loubser from the Faculty of Humanities for her valued critique and peer comments on the chemistry and analytical content, including Sandra Markgraaf, the University of Pretoria Museum Art Conservator for the preparation of the graphite bars for the selective samples chosen by the Curator of the Mapungubwe Gold Collection from the University of Pretoria Museums, in South Africa. Thanks to the Manheim Museum; the University of Pretoria Museums, the Rijksmuseum Amsterdam, and the Museums of Segovia and Belles Arts de Castelló, as well as the Servei d'Investigació Arqueològica Municipal de València (SIAM).

Appendix A. Supplementary data

Supplementary data to this article can be found online at https://doi.org/10.1016/j.microc.2023.108661.

References

[1] M.J. Aitken, Science-Based Dating in Archaeology, Longman, New York, 1990.
[2] M.A. Geyh, H. Schleicher (Eds.), Absolute Age Determination, Springer Berlin Heidelberg, Berlin, Heidelberg, 1990.
[3] G. Artioli, Scientific Methods and Cultural Heritage, Oxford Univ. Press, 2010.
[4] S. Reich, G. Leitus, S. Shalev, Measurement of corrosion content of archaeological lead artifacts by their Meissner response in the superconducting state; a new dating method, New J. Phys. 5 (2003) 99.1–99.9.
[5] O. Eugster, Dating gold artifacts applications for noble gas analysis of gold, Gold Bull. 29 (1996) 101–104.
[6] O. Eugster, J. Kramers, U. Krähenbühl, Detecting forgeries among ancient gold objects using the U, Th-^{4}He dating method, Archaeometry 51 (2009) 672–681.
[7] A. Doménech-Carbó, M.T. Doménech-Carbó, M.A. Peiró-Ronda, Dating archaeological lead artifacts from measurement of the corrosion content using the voltammetry of microparticles, Anal. Chem. 83 (2011) 5639–5644.
[8] A. Doménech-Carbó, M.T. Doménech-Carbó, S. Capelo, T. Pasíes-Oviedo, I. Martínez-Lázaro, Dating archaeological copper/bronze artifacts using the voltammetry of microparticles, Angew. Chem. Int. Ed. 53 (2014) 9262–9266.
[9] A. Doménech-Carbó, M.T. Doménech-Carbó, J. Redondo-Marugán, L. Osete-Cortina, J. Barrio, A. Fuentes, M.V. Vivancos-Ramón, W. Al-Sekhaneh, B. Martínez, I. Martínez-Lázaro, T. Pasíes-Oviedo, Electrochemical characterization and dating of archeological leaded bronze objects using the voltammetry of immobilized particles, Archaeometry 60 (2018) 308–324.
[10] A. Doménech-Carbó, F. Scholz, Electrochemical age determinations of metallic specimens – *the utilization of the corrosion clock*, Acc. Chem. Res. 52 (2019) 400–406.
[11] A. Doménech-Carbó, F. Scholz, M.T. Doménech-Carbó, J. Piquero-Cilla, N. Ontoya, T. Pasíes-Oviedo, M. Gozalbes, M. Melchor-Montserrat, A. Oliver, Dating of archaeological gold by means of solid state electrochemistry, ChemElectroChem 5 (2018) 2113–2217.
[12] A. Doménech-Carbó, F. Scholz, M. Brauns, S. Tiley-Nel, A. Oliver, G. Aguilella, N. Montoya, M.T. Doménech-Carbó, Dating archaeological gold from electrochemical monitoring of desilvering/decuprification processes, Electrochim. Acta 337 (2020), 135759.
[13] I. Tissot, L.G. Troalen, M. Manso, M. Ponting, M. Radtke, U. Reinholz, M. A. Barreiros, G. Shaw, M.L. Carvalho, M.F. Guerra, A multi-analytical approach to gold in Ancient Egypt: studies on provenance and corrosion, Spectrochim. Acta B 108 (2015) 75–82.
[14] M. Radtke, G. Buzanich, A. Guilherme, U. Reinholz, H. Riesemeier, O. Scharf, P. Scholz, M.F. Guerra, Double dispersive X-Ray fluorescence (D2XRF) based on an Energy Dispersive pnCCD detector for the detection of platinum in gold, Microchem. J. 125 (2016) 56–61.

[15] I. Ortega-Feliu, S. Scrivano, B. Gómez-Tubío, F.J. Ager, M.L. de la Bandera, M. A. Respaldiza, A.D. Navarro, C. San Martín, Technical characterization of the necklace of El Carambolo hoard (Camas, Seville, Spain), Microchem. J. 139 (2018) 401–409.

[16] A. Manas, Gold's red shift: colorimetry of multiple reflections in grooves, Gold Bull. 53 (2020) 147–158.

[17] E.S. Blakelock, Never judge a gold object by its surface analysis: a study of surface phenomena in a selection of gold objects from the Staffordshire Hoard, Archaeometry 58 (2016) 919–929.

[18] F. Scholz, B. Meyer, Voltammetry of solid microparticles immobilized on electrode surfaces, in Electroanalytical Chemistry, A Series of Advances. A.J. Bard, I. Rubinstein, Eds., Marcel Dekker, New York, 1998, vol. 20, pp. 1−86.

[19] F. Scholz, U. Schröder, R. Gulabowski, A. Doménech-Carbó, Electrochemistry of Immobilized Particles and Droplets, 2nd ed., Springer, Berlin-Heidelberg, 2014.

[20] A. Doménech-Carbó, M. T. Doménech-Carbó, V. Costa, Electrochemical Methods in Archaeometry, Conservation and Restoration (Monographs in Electrochemistry series, F. Scholz, Ed.), Springer, Berlin-Heidelberg, 2009.

[21] A. Doménech-Carbó, J. Labuda, F. Scholz, Electroanalytical chemistry for the analysis of solids: characterization and classification (IUPAC Technical Report), Pure Appl. Chem. 85 (2013) 609–631.

[22] A. Doménech-Carbó, M.T. Doménech-Carbó, Electroanalytical techniques in archaeological and art conservation, Pure Appl. Chem. 90 (2018) 447–462.

[23] F. Scholz, U. Schröder, S. Meyer, K.Z. Brainina, N.F. Zakharchuk, N.V. Sobolev, O. A. Kozmenko, The electrochemical response of radiation defects of non-conducting materials An electrochemical access to age determinations, J. Electroanal. Chem. 385 (1995) 139–142.

[24] A. Doménech-Carbó, Dating –An analytical task-, ChemTexts 1 (2015) 5.

[25] A. Doménech-Carbo, Electrochemical dating: a review, J. Solid State Electrochem. 21 (7) (2017) 1987–1998.

[26] N.D. Meeks, Tin-rich surfaces on bronze – Some experimental and archaeological considerations, Archaeometry 28 (1986) 133–162.

[27] C. Chiavari, K. Rahmouni, H. Takenouti, S. Joiret, P. Vermaut, L. Robbiola, Composition and electrochemical properties of natural patinas of outdoor bronze monuments, Electrochim. Acta 52 (2007) 7760–7769.

[28] R. Borges, L. Alves, R.J.C. Silva, M.F. Araújo, A. Candeias, V. Corregidor, P. Valério, P. Barrulas, Investigation of surface silver enrichment in ancient high silver alloys by PIXE, EDXRF, LA-ICP-MS and SEM-EDS, Microchem. J. 131 (2017) 103–111.

[29] E. Ottenwelter, V. Costa, Evidence of metallic plating on archaeological artefacts by voltammetry of microparticles, Archaeometry 57 (2015) 497–504.

[30] E. Caponetti, F. Armetta, L. Brusca, D.C. Martino, M.L. Saladino, S. Ridolfi, G. Chirco, M. Berrettoni, P. Conti, N. Bruno, S. Tusa, A multivariate approach to the study of orichalcum ingots from the underwater Gela's archaeological site, Microchem. J. 135 (2017) 163–170.

[31] M.T. Domenech-Carbo, F. Di Turo, N. Montoya, F. Catalli, A. Domenech-Carbo, C. De Vito, FIB-FESEM and EMPA results on Antoninianus silver coins for manufacturing and corrosion processes, Sci. Rep. 8 (2018) 10676.

[32] L. Fabrizi, F. Di Turo, L. Medeghini, M. Di Fazio, F. Catalli, C. De Vito, The application of non-destructive techniques for the study of corrosion patinas of ten Roman silver coins: the case of the medieval *Grosso Romanino*, Microchem. J. 145 (2019) 419–427.

[33] D. Berger, M. Brauns, G. Brügmann, E. Pernicka, N. Lockhoff, Revealing ancient gold parting with silver and copper isotopes: implications from cementation experiments and for the analysis of gold artefacts, Archaeol. Anthropol. Sci. 13 (2021) 143.

[34] L. Robbiola, L.-P. Hurtel, Standard nature of the passive layers of buried archaeological bronze - The example of two Roman half-length portraits, in: I. MacLeod, S. Pennec, L. Robbiola (Eds.), METAL 95, James & James Science Publ, London, 1997, pp. 109–117.

[35] J.-M. Welter, The zinc content of brass: a chronological indicator, Techné 18 (2003) 27–36.

[36] A. Doménech-Carbó, M.T. Doménech-Carbó, I. Martínez-Lázaro, Layer-by-layer identification of copper alteration products in metallic works of art using the voltammetry of microparticles approach, Anal. Chim. Acta 680 (2010) 1–9.

[37] A. Doménech-Carbó, M. Donnici, C. Álvarez-Romero, S. Daniele, M.T. Doménech-Carbó, Multiple-scan voltammetry of immobilized particles of ancient copper/bronze coins, J. Solid State Electrochem. 25 (2021) 195–206.

[38] A. Domenech-Carbo, J.M. del Hoyo-Melendez, M.T. Domenech-Carbo, J. Piquero-Cilla, Electrochemical analysis of the first Polish coins using voltammetry of immobilized particles, Microchem. J. 130 (2017) 47–55.

[39] S. Capelo, O.M. Homem, J. Cavalheiro, I.T.E. Fonseca, Linear sweep voltammetry: a cheap and powerful technique for the identification of the silver tarnish layer constituents, J. Solid State Electrochem. 17 (2013) 223–234.

[40] X. Ferragud, J. Piquero-Cilla, M.T. Doménech-Carbó, V. Guerola-Blay, X. Company, A. Doménech-Carbó, Electrochemical analysis of gildings in Valencia Altarpieces: a cross-age study since 15th until 20th century, J. Solid State Electrochem. 21 (2017) 1477–1487.

[41] B. Martínez, J. Piquero-Cilla, N. Montoya, M.T. Doménech-Carbó, A. Doménech-Carbó, Electrochemical analysis of gold embroidery threads from archaeological textiles, J. Solid State Electrochem. 22 (2018) 2205–2215.

[42] J. Herrera-Gallego, C.E. Castellano, A. Calandra, A.J. Arvia, The electrochemistry of gold in acid aqueous solutions containing chloride ions, J. Electroanal. Chem. 66 (1975) 207–230.

[43] J. Desilvestro, M.J. Weaver, Surface structural changes during oxidation of gold electrodes in aqueous media as detected using surface-enhanced Raman spectroscopy, J. Electroanal. Chem. 209 (1986) 377–386.

[44] L.D. Burke, P.F. Nugent, The electrochemistry of gold: I the redox behaviour of the metal in aqueous media, Gold Bull. 30 (1997) 43–53.

[45] O. Diaz-Morales, F. Calle-Vallejo, C. de Munck, M.T. Koper, Electrochemical water splitting by gold: evidence for an oxide decomposition mechanism, Chem. Sci. 4 (2013) 2334–2343.

[46] U. Hasse, H. Wulff, C.A. Helm, F. Scholz, Formation of gold surfaces with a strongly preferred {100}-orientation, J. Solid State Electrochem. 17 (2013) 3047–3053.

[47] L.D. Burke, A.P. O'Mullane, Generation of active surface states of gold and the role of such states in electrocatalysis, J. Solid State Electrochem. 4 (2000) 285–297.

[48] A. Nowicka, U. Hasse, G. Sievers, M. Donten, Z. Stojek, S. Fletcher, F. Scholz, Selective knockout of gold active sites, Angew. Chem. Int. Ed. 49 (2010) 3006–3009.

[49] F. Scholz, G. Lopez de Lara-Gonzalez, L.M. de Carvalho, L. Hilgemann, K. Z. Brainina, H. Kahlert, R.S. Jack, D.T. Minh, Indirect electrochemical sensing of radicals and radical scavengers in biological matrices, Angew. Chem. Int. Ed. 46 (2007) 8079–8081.

[50] U. Hasse, K. Fricke, D. Dias, G. Sievers, H. Wulff, F. Scholz, Grain boundary corrosion of the surface of annealed thin layers of gold by OH· radicals, J. Solid State Electrochem. 16 (2012) 2383–2389.

[51] A. Nowicka, U. Hasse, M. Hermes, F. Scholz, Hydroxyl radicals attack metallic gold, Angew. Chem. Int. Ed. 49 (6) (2010) 1061–1063.

[52] S. Cherevko, N. Kulyk, C.-H. Chung, Utilization of surface active sites on gold in preparation of highly reactive interfaces for alcohols electrooxidation in alkaline media, Electrochim. Acta 69 (2012) 190–196.

[53] R.L. Doyle, M.E.G. Lyons, The mechanism of oxygen evolution at superactivated gold electrodes in aqueous alkaline solution, J. Solid State Electrochem. 18 (2014) 3271–3286.

[54] S. Woodbourne, M. Pienaar, S. Tiley-Nel, The dating of the gold graves from Mapungubwe Hill, J. African Archaeol. 7 (2009) 95–101.

[55] S. Tiley-Nel, A. Botha, Conservation of the Mapungubwe gold collection, J. Ite. Cons. 36 (2013) 65–80.

[56] J.L. Ruvalcaba, L. Torres, E. Ortíz, Artifact rich gold surfaces: depletion gilding or natural surface corrosion? Study of corrosion and oxidation of gold alloys, in: A. Perea, I. Montero, O. García-Vuelta (Eds.), Tecnología del Oro Antiguo: Europa y América, Anejos de España XXXII, Madrid CSIC, 2004, pp. 41–48.

[57] J. Tate, Some problems in analysing museum material by nondestructive Surface sensitive techniques, Nucl. Inst. Methods B 14 (1) (1986) 20–23.

[58] D.A. Scott, The deterioration of gold alloys and some aspects of their conservation, Stud. Conserv. 28 (1983) 194–203.

[59] I. Tissot, L.G. Troalen, M. Manso, M. Ponting, M. Radtke, U. Reinholz, M. A. Barreiros, I. Shaw, M.L. Carvalho, M.F. Guerra, A multi-analytical approach to gold in ancient Egypt: studies on provenance and corrosion, Spectrochim. Acta B At. Spectrosc. 108 (2015) 75–82.

[60] C.N. Zwicky-Sobczyk, W.B. Stern, X-ray fluorescence and density measurements on surface-treated Roman silver coins, Archaeometry 39 (2) (1997) 393–405.

[61] R. Linke, M. Schreiner, G. Demortier, The application of photon, electron and proton induced X-ray analysis for the identification and characterization of medieval silver coins, Nucl. Inst. Methods Phys. Res. B 226 (2004) 172–178.

[62] A.I. Moreno-Suárez, F.J. Ager, S. Scrivano, I. Ortega-Feliu, B. Gómez-Tubío, M. A. Respaldiza, First attempt to obtain the bulk composition of ancient silver – copper coins by using XRF and GRT, Nucl. Inst. Methods Phys. Res. B 358 (2015) 93–97.

[63] J.M. Hoyo-Meléndez, P. Świt, M. Matosz, M. Woźniak, A. Klisińska-Kopacz, Ł. Bratasz, Micro-XRF analysis of silver coins from medieval Poland, Nucl. Inst. Methods Phys. Res. B 349 (2015) 6–16.

[64] C.J. Raub, Metallurgy of gold and silver in prehistoric times, in: G. Morteani, J. P. Northover (Eds.), Prehistoric gold in Europe: mines, metallurgy and manufacture, Kluwer Academic, Dordrecht, 1995, pp. 243–259.

[65] G. Lehrberger, C.J. Raub, A look into the interior of Celtic gold coins, in: G. Morteani, J.P. Northover (Eds.), Prehistoric gold in Europe: mines, metallurgy and manufacture, Kluwer Academic, Dordrecht, 1995, pp. 341–355.

[66] P. Möller, Electrochemical corrosion of natural gold alloys, in, in: G. Morteani, J. P. Northover (Eds.), Prehistoric gold in Europe: mines, metallurgy and manufacture, Kluwer Academic, Dordrecht, 1995, pp. 356–367.

[67] J.M. Poate, Diffusion and Reactions in Gold Films A review of fundamental aspects, Gold Bull. 14 (1981) 2–11.

[68] H.-J. Seol, J.-H. Park, R.-M. Ku, M.-G. Park, Y.H. Kwon, H.I. Kim, Age-hardening by miscibility limit in a multi-purpose dental gold alloy containing platinum, Gold Bull. 43 (2010) 42–48.

[69] H. Hieber, K. Pape, Ageing of thin gold films, Gold Bull. 15 (1982) 90–100.

[70] G. Hultquist, Surface enrichment of low gold alloys, Gold. Bull. 18 (1985) 53–57.